Lawrence Berkeley National Laboratory

Title

Revealing the Distribution of Metal Carboxylates in Oil Paint from the Micro- to Nanoscale

Permalink

https://escholarship.org/uc/item/82r2763m

Journal

Angewandte Chemie International Edition, 58(34)

ISSN

1433-7851

Authors

Ma, Xiao
Beltran, Victoria
Ramer, Georg
et al.

Publication Date

2019-08-19

DOI

10.1002/anie.201903553

Peer reviewed

Revealing the distribution of metal carboxylates in oil paint from the micro- to nanoscale

Xiao Ma,

Scientific Research Department, Division of Conservation, National Gallery of Art, 2000B South Club Drive, Landover, MD 20785 (USA)

Victoria Beltran[+],

IPANEMA, CNRS, ministère de la Culture et de la Communication Université de Versailles Saint-Quentin-en-Yvelines, USR 3461, Université Paris-Saclay, 91128 Gif-sur-Yvette (France)

Georg Ramer[+],

Nanoscale Device Characterization Division, Physical Measurement Laboratory, National Institute of Standards and Technology, 100 Bureau Drive, Gaithersburg, MD 20899 (USA); Maryland Nanocenter, University of Maryland, College Park, MD 20742 (USA)

Georges Pavlidis,

Nanoscale Device Characterization Division, Physical Measurement Laboratory, National Institute of Standards and Technology, 100 Bureau Drive, Gaithersburg, MD 20899 (USA)

Dilworth Y. Parkinson,

Advanced Light Source, Lawrence Berkeley National Laboratory, 1 Cyclotron Rd., Berkeley, CA 94720 (USA)

Mathieu Thoury,

IPANEMA, CNRS, ministère de la Culture et de la Communication Université de Versailles Saint-Quentin-en-Yvelines, USR 3461, Université Paris-Saclay, 91128 Gif-sur-Yvette (France)

Tyler Meldrum,

Department of Chemistry, The College of William & Mary, 540 Landrum Drive, Williamsburg, VA 23188 (USA)

Andrea Centrone,

Nanoscale Device Characterization Division, Physical Measurement Laboratory, National Institute of Standards and Technology, 100 Bureau Drive, Gaithersburg, MD 20899 (USA)

Barbara H. Berrie

Scientific Research Department, Division of Conservation, National Gallery of Art, 2000B South Club Drive, Landover, MD 20785 (USA)

Abstract

andrea.centrone@nist.gov; B-BERRIE@nga.gov.

[+]These authors contributed equally to this work.

Oil paints comprise pigments, drying oils and additives that together confer desirable properties, but can react to form metal carboxylates (soaps) that may damage artworks over time. To obtain information on soap formation and aggregation, we introduce a new tapping-mode measurement paradigm for the photothermal induced resonance (PTIR) technique that enables nanoscale IR spectroscopy and imaging on highly heterogenous and rough paint thin sections. PTIR is used in combination with µ-computed tomography and IR microscopy to determine the distribution of metal carboxylates in a 23-year old oil paint of known formulation. Results show that heterogeneous agglomerates of Al-stearate and a Zn-carboxylate complex with Zn-stearate nano-aggregates in proximity are distributed randomly in the paint. The gradients of zinc carboxylates are unrelated to the Al-stearate distribution. These measurements open a new chemically sensitive nanoscale observation window on the distribution of metal soaps that can bring insights for understanding soap formation in oil paint.

Graphical Abstract
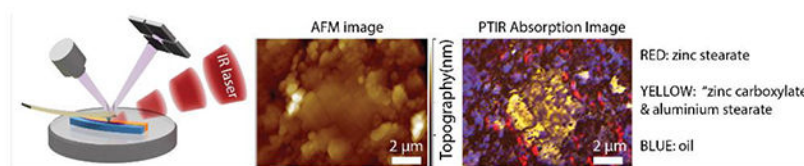
IR nanoscopy of paints:

A new implementation of a compositionally sensitive AFM-based method (PTIR) reveals metal-soaps (metal carboxylate) composition and heterogeneous distribution in naturally aged paints.

Keywords

Metal Carboxylates; PTIR; IR Spectroscopy; Analytical Methods; Art Conservation

Oil paints have long been used to create artworks and find application as protective layers on wood or metals. They offer desirable aesthetic and physical characteristics. However, one common, typically ongoing reaction between metal ions (from metal-containing pigments) and free fatty acids (from hydrolyzed triglycerides of the oil binding medium and additives) leads to the formation of metal carboxylates (soaps). The formation of zinc and lead carboxylates appears to be a general process occurring in oil paints that lead to spalling, cracking, and the development of pimpled surfaces on artworks.[1] Metal soaps have also been identified in paints containing copper, cadmium and manganese.[2] The physical deterioration caused by soap aggregation is a challenge for art conservation. Currently, much research [1b, 3] is devoted to identifying the species involved and understanding the sequence of processes that lead to those adverse effects. For example, paint additives such as fats and metal stearates used to control paints' rheological properties and to promote pigment wetting can exacerbate soap formation by reacting with the pigments.[3d, 4] However, not enough is known of soap formation and aggregation, to mitigate their effects and propose effective conservation treatments.

In this work, we report a novel tapping-mode implementation scheme for the photothermal induced resonance (PTIR) [5] technique, a nano-infrared spectroscopy method that uses an atomic force microscope (AFM) probe to overcome the light diffraction limit. This new implementation, better adapted to measure highly heterogeneous and rough paint samples, is used here to study in detail the distribution of metal soaps in samples (hereafter paint outs) of known average composition prepared at the Grumbacher paint factory in 1995. Zinc-containing Pre-tested Soft Titanium White (P250) paint was chosen. This 23-year old, naturally-aged paint-out is completely analogous to an oil painting. It was chosen because it has not undergone any conservation treatment or artificial aging, thereby offering a well-characterized system for studying the development of soaps in real works of art.

PTIR reveals a complex distribution of metal carboxylates, which is heterogenous at the nanoscale. For example, it can detect the three distinct metal carboxylates within and around a single agglomerate of the aluminium stearate additive. Since, as for most AFM techniques, PTIR has typically a low throughput, here synchrotron-based micro-computed tomography (μ-CT) and Fourier transform infrared (FTIR) micro spectroscopy are also employed to assess compositional gradients across the whole paint film. Together these measurements offer new insights and further current efforts [6] to better understand soap formation and aggregation processes in artworks.

The initial nominal mass fractional composition of the paint (P250) is: drying oils ($\approx$ 27 %), titanium white (anatase, $\approx$ 23 %), zinc white ($\approx$ 46 %), and aluminium tristearate (Al-stearate, $\approx$ 4 %) added to counteract pigment settling in the paint tube and provide thixotropic behaviour. The paint was applied as a $\approx$ 125 μm thick film onto a commercial zinc white oil-primed support, rather than an inert support. A cross-section sample of the paint-out (Figure 1 and Figure S1) has 6 layers, labelled I to VI, whose composition was identified using a combination of analytical techniques confirming the expected formulation. See Supporting Information (Figure S1–S4) for the full characterization and further details of the components. Hereafter, we focus on the metal carboxylates, primarily in the paint layer VI.

Transmission μ-FTIR spectra of powdered samples obtained from the priming layers III and IV and from the paint layer VI show similarities and notable differences (see Figure S5). In the priming layers III and IV, a broad band at $\approx$ 1590 cm^{-1} v_{as} (COO$^-$) is like the broad peak of zinc soaps observed in nineteenth- and twentieth-century paintings.[3d, 3f, 4a] This feature has been attributed to a mixture of zinc carboxylates with different molecular weights,[2] and a useful hypothesis suggests it is due to the formation of an ionomeric phase where zinc ions are an integrated part of a cured oil network that forms by metal ion migration and reaction with a oxidized linoxyn film.[3f] A broad carboxylate absorption also develops in model complexes obtained by reacting zinc acetate and ethyl linoleate, suggesting that soap formation in oil paint involves polyunsaturated fatty acids which, however, oxidize rapidly and are not present in historical paints. [7] Hereafter, we refer to this feature in the IR spectra as "zinc carboxylate". In the paint layer, peaks at 1540 cm^{-1} (v_{as} (COO$^-$), sharp), 1464 cm^{-1} (δ (CH$_2$)) and 1398 cm^{-1} (v_s (COO$^-$)) can be attributed to zinc stearate. [3b, 3e] The broad band centered at $\approx$ 1587 cm^{-1} derives from a small contribution of Al-stearate (v_{as}

$(COO^-) \approx 1588$ cm^{-1}, a narrow peak) and from a large contribution of "zinc carboxylate" (v_{as} $(COO^-) \approx 1590$ cm^{-1}, a broad peak).

Hydrolysis of Al-stearate added to the paint leads to formation of free stearic acid which can react with zinc oxide to form zinc stearate (ZnSt$_2$).[3d, 4a] Gabrieli et al. reported that large amounts of ZnSt$_2$ had formed in a mid-20th century oil painting due to the presence of Al-stearate.[4b] Below, we show that the distribution of zinc carboxylates in association with Al-stearate is more complex and heterogenous at the nanoscale than previously recognized.

Contrast in μ-CT images of an unembedded sample from P250 (Figure 1, C, D) shows low density (i.e., dark) regions dispersed throughout the paint film that correlate with low-atomic weight, Al-rich circular regions identified in the backscattered electron (BSE) image and Al-EDX map (Figure 1, A, B). Rotation of the μ-CT scan (Movie S1) reveals these regions are not spherical, but irregularly shaped, with lengths generally less than 10 μm (see 3-D reconstruction in Figure 1 E). The distribution of absorption coefficients of the paint layer VI is plotted in Figure S6. Thresholding shows the Al-rich agglomerates are distributed randomly throughout the paint layer (Figure 1 D, E and Movie S2), meaning that cross sections and thin sections are representative of the paint film. No gradients, settling, or zoning of the Al-rich agglomerates are evident, in contrast to previous observations.[3d, 4a] EDX analysis of a low-density agglomerate, on a ≈ 200 nm thick cross section (Figure S7), indicates that it contains both Al and Zn.

FTIR microscopy and PTIR nanoscopy were employed to investigate composition gradients and chemical heterogeneity in the paint film at the micro- and nanoscale, respectively. PTIR enables nanoscale IR characterization using an AFM probe as a near-field mechanical detector.[5] In PTIR, also known as AFM-IR, a pulsed wavelength-tunable laser illuminates a portion of the sample centred around the AFM tip. Following absorption of a light pulse, the sample heats and expands rapidly,[8] kicking the AFM cantilever into oscillation with an amplitude proportional to the absorbed energy.[9] The PTIR signal proportionality to the sample absorption coefficient, as in FTIR, enables identification of materials and chemical groups, leading to broad applications in materials science and biology.[8, 10] Related to art conservation, PTIR was used to characterize parchment degradation [11] and the UV-induced, accelerated degradation of linseed oil in titanium white paints.[12] A key characteristic that distinguishes PTIR from other chemically-sensitive AFM techniques is its ability to probe the composition in samples even thicker than 1 μm.[13] Since the PTIR spatial resolution depends in part on the sample thermomechanical properties, the sample stratification and its thickness,[5, 14] the best spatial resolution is obtained for thin (< 500 nm) samples that are vertically homogeneous. While PTIR experiments are typically carried out in contact-mode, here we employ tapping mode with a novel heterodyne detection scheme (Figure 2 A, B) where the tapping motion of the cantilever is mixed with the sample expansion due to non-linear tip-sample interactions.[15] Critically, this implementation is better adapted to analyze the chemically heterogeneous and topographically varied paint thin sections studied here. In particular, tapping-mode PTIR signal transduction is much less sensitive to heterogeneity in the sample mechanical properties than resonance-enhanced contact-mode operation.[6] In practice, a piezo actuator drives the cantilever at its second mechanical resonance (f$_2$ ≈ 1550 kHz), the PTIR signal is demodulated at its first

mechanical resonance ($f_1 \approx 250$ kHz) while pulsing the IR laser with a repetition rate f_L = f_2 - $f_1 \approx 1300$ kHz. With respect to our previous tapping-mode PTIR implementation[6, 16] (signal demodulated at f_2), demodulating the signal at f_1, enables the acquisition of better quality tapping-mode PTIR spectra, which is key for chemical identification. This novel technical advance effectively broadens PTIR application horizon to include samples that otherwise would be difficult to characterize in contact-mode, such as the samples relevant for paint degradation and other art conservation challenges.

PTIR maps and spectra (Figure 2) were obtained on a ≈ 200 nm thick section to identify the composition and the distribution of the Al-rich low-density agglomerates identified in Figure 1. Representative spectra (points 1-3, Figure 2 C, F) show that the agglomerate consists of Al-stearate (narrow peak at 1590 cm^{-1}), "zinc-carboxylate" (broad peak at ≈ 1590 cm^{-1}), oil (1742 cm^{-1}) and only a small amount of ZnSt$_2$ (shoulder at 1540 cm^{-1}). The large variation of the relative intensity of the 1590 cm^{-1} peak indicates that the proportion of Al-stearate within the agglomerate varies greatly. PTIR absorption maps at the above characteristic frequencies (marker bands) reveal the distribution of oil (Figure 2 E), "zinc carboxylate" plus Al-stearate (Figure 2 F) and ZnSt$_2$ (Figure 2 G). The latter shows nano-aggregates of ZnSt$_2$ both at the rim of Al-rich agglomerate and in the paint film. The typical size of the ZnSt$_2$ clusters ranges from 100 nm to 400 nm, too small to be observed using μ-FTIR mapping.[4b] No concentration gradient of ZnSt$_2$ is observed at this scale. A representative spectrum from these areas (point 5, Figure 2 C, G) shows strong 1540 cm^{-1} absorption (ZnSt$_2$, v_{as} (COO$^-$)) and relatively weaker peak at 1742 cm^{-1} indicating a lower fraction of oil at that site. PTIR overlay images (Figure 2 H, I) show that the aluminium stearate-rich agglomerates and the nearest ZnSt$_2$ clusters are separated by a thin layer of oil. The likely explanation is that free stearic acid molecules migrate from the aluminium stearate-rich agglomerates through the oil to react with zinc oxide in the film.

The PTIR spectrum from an area with strong absorption at 1590 cm^{-1} outside the aluminium stearate-rich agglomerate (point 4, Figure 2 C, F) has broad bands at ≈ 1594 cm^{-1} (v_{as} (COO$^-$)) and 1410 cm^{-1} (v_s (COO$^-$)) similar to those observed in real paintings [3d, 4a] and in the priming layers (Figure S5). The phase characterized by this broad carboxylate peak derives from the reaction between zinc ions and oil. It is interesting to note this "zinc carboxylate" seems to be in localized areas and is not continuous throughout the paint film.

The high sensitivity and spatial resolution of PTIR allows disentangling the composition of paints and revealing for the first time that the agglomerates derived from the Al-stearate additive contain at least three metal carboxylates and oil. Unexpectedly, the zinc ions detected by EDX (Figure S7) belong mainly to "zinc carboxylate" (Figure 2 C, F), demonstrating these species can intermix.

Although of lower spatial resolution, the higher measurement throughput of μ-FTIR mapping enables assessing the distribution and composition gradients in the whole paint film. Integrated absorption intensity maps of a thin section (6 μm) of the paint-out are shown in Figure S9. Notably, both ZnSt$_2$ (1540 cm^{-1}, Figure S9 C) and "zinc carboxylate" (1587 cm^{-1}, Figure S9 D) are present throughout the paint layer but with increasing concentration towards bottom and top of the layer, respectively. Deconvolution of the two carboxylate

peaks in representative small areas (regions of interest - ROI 3 to 7 in Figure S9 C) shows that the ratio of "zinc carboxylate"/ZnSt$_2$ peak area decreases gradually from the top of the film (ROI 3) to the bottom (ROI 7), see Figure 3 (inset figure).

By normalizing the spectra from all ROIs to the CH$_2$ asymmetric stretching peak at $\approx$ 2918 cm^{-1} (Figure 3), two observations are possible. First, the v_{as} (CH$_2$) at 2918 cm^{-1} (characteristic of aliphatic chains in trans conformation) shows a shoulder at $\approx$ 2926 cm^{-1} (characteristic of conformational disordered aliphatic chains) [17] that increases in intensity from the bottom to the top of the paint layer. Second, v_{as} (CH$_3$) peak ($\approx$ 2952 cm^{-1}) also increases in intensity from the bottom to the top of the paint film. This suggests that the aliphatic chains towards the top of the paint film are both shorter and more conformationally disordered, correlating well with the observed distribution of the "Zn carboxylate" phase.

The µ-FTIR spectrum of Grumbacher P250 expressed from a tube opened for the first time to perform the analysis (Figure S10) is similar to that of the cured paint layer (Figure S5) suggesting that ZnSt$_2$ and "zinc carboxylate" form inside the tube or even during the mixing process in the factory. The gradient in their relative concentrations in the cured paint film must, however, develop after the paint has been applied onto the canvas.

The development of ZnSt$_2$ gradients has been postulated to arise from ZnSt$_2$ migration towards [3d] or preferential formation at the bottom of paint films.[18] Although a gradient of ZnSt$_2$ is also observed in this work, no compelling evidence was obtained to distinguish between the two hypotheses. However, since the aluminium stearate-rich agglomerates are evenly distributed throughout the paint film, as shown from µ-CT, the zinc soaps gradients must form independently from Al-stearate. We hypothesize that from the top to the bottom of the paint film, the relative amount of free saturated fatty acids (contributing to ZnSt$_2$) increases with respect to the amount of polyunsaturated fatty acids and polymerized oil network (contributing to "zinc carboxylate").

The aged paint used in this study does not yet show signs of physical deterioration, however, we anticipate if hydrolysis of Al-stearate progresses, the concentration gradients of ZnSt$_2$ will become more pronounced, eventually leading to spalling.

The techniques used here provide chemical information over many length scales adding significantly to our knowledge of metal-carboxylate formation and distribution in paint. IR nanoscopy reveals for the first time that "zinc carboxylate" and Al-stearate are finely intermixed within aluminium stearate-rich agglomerates in oil paint. Additionally, ZnSt$_2$ nano-aggregates are found both near the rim of the aluminium stearate-rich agglomerates and dispersed throughout the paint. µ-FTIR mapping reveals expected ZnSt$_2$ and "zinc carboxylate" gradients. The findings are valuable for better understanding the relationship between the distribution of soaps and long-term changes in paint films that can ultimately lead to paint deterioration. Particularly, the novel PTIR tapping-mode implementation presented here is better adapted to measure highly heterogeneous and topographically varying samples. Consequently, we believe that this PTIR measurement modality will find broad application in art conservation and for the characterization of a wider variety of material systems. The synergy of the methods used here can be applied broadly to address

issues that challenge art conservation and other fields where materials with multiscale chemical heterogeneity are important, such as biomedicine and energy storage.

Supplementary Material

Refer to Web version on PubMed Central for supplementary material.

Acknowledgements

References

[1]. a) Osmond G, Keune K, Boon J, AICCM Bulletin 2005, 29, 37;b) Casadio F, Keune K, Noble P, Loon AV, Hendriks E, Centeno SA, Osmond G, in Cultural Heritage Science, Springer, 2019.

[2]. Mazzeo R, Prati S, Quaranta M, Joseph E, Kendix E, Galeotti M, Anal. Bioanal. Chem 2008, 392, 65. [PubMed: 18454281]

[3]. a) Boon JJ, van der Weerd J, Keune K, Noble P, Wadum J, in 13th Triennial ICOM-CC Meeting, Vol. 1 (Ed.: Vontobel R), James & James, Rio De Janeiro, 2002, pp. 401;b) Robinet L, Corbeil M-C, Stud. Conserv 2003, 48, 23;c) Maines CA, Rogala D, Lake S, Mecklenburg M, MRS Proceedings 2011, 1319, mrsf10;d) Osmond G, Boon JJ, Puskar L, Drennan J, Appl. Spectrosc 2012, 66, 1136; [PubMed: 23031696] e) Otero V, Sanches D, Montagner C, Vilarigues M, Carlyle L, Lopes JA, Melo MJ, Raman Spectrosc J. 2014, 45, 1197;f) Hermans JJ, Keune K, van Loon A, ledema PD, J. Anal. At. Spectrom 2015, 30, 1600;g) Catalano J, Murphy A, Yao Y, Yap GPA, Zumbulyadis N, Centeno SA, Dybowski C, Dalton Trans. 2015, 44, 2340; [PubMed: 25534137] h) Chen-Wiegart Y.-c. K., Catalano J, Williams GJ, Murphy A, Yao Y, Zumbulyadis N, Centeno SA, Dybowski C, Thieme J, Sci. Rep 2017, 7, 11656; [PubMed: 28912460] i) Catalano J, Murphy A, Yao Y, Zumbulyadis N, Centeno SA, Dybowski C, Solid State Nucl. Magn. Reson 2018, 89, 21. [PubMed: 29277314]

[4]. a) Osmond G, in Issues in Contemporary Oil Paint (Eds.: van den Berg KJ, Burnstock A, de Keijzer M, Krueger J, Learner T, de Tagle A, Heydenreich G), Springer International Publishing, Cham, 2014, pp. 263;b) Gabrieli F, Rosi F, Vichi A, Cartechini L, Pensabene Buemi L, Kazarian SG, Miliani C, Anal. Chem 2017, 89, 1283. [PubMed: 28035811]

[5]. a) Centrone A, Annu. Rev. Anal. Chem 2015, 8, 101;b) Dazzi A, Prater CB, Chem. Rev 2017, 117, 5146. [PubMed: 27958707]

[6]. Wieland K, Ramer G, Weiss VU, Allmaier G, Lendl B, Centrone A, Nano Res. 2019, 12, 197.

[7]. MacDonald MG, Palmer MR, Suchomel MR, Berrie BH, ACS Omega 2016, 1, 344. [PubMed: 31457132]

[8]. Chae J, An S, Ramer G, Stavila V, Holland G, Yoon Y, Talin AA, Allendorf M, Aksyuk VA, Centrone A, Nano Lett. 2017, 17, 5587. [PubMed: 28770607]

[9]. Dazzi A, Glotin F, Carminati R, J. Appl. Phys 2010, 107, 124519.

[10]. a) Katzenmeyer AM, Canivet J, Holland G, Farrusseng D, Centrone A, Angew. Chem. Int. Ed 2014, 53, 2852;b) Chae J, Dong O, Huang J, Centrone A, Nano Lett. 2015, 15, 8114; [PubMed: 26528710] c) Morsch S, Liu Y, Lyon SB, Gibbon SR, ACS Appl. Mater. Interfaces 2016, 8, 959; [PubMed: 26694687] d) Giliberti V, Badioli M, Nucara A, Calvani P, Ritter E, Puskar L, Aziz EF, Hegemann P, Schade U, Ortolani M, Baldassarre L, Small 2017, 13, 1701181;e) Ramer G, Ruggeri FS, Levin A, Knowles TPJ, Centrone A, ACS Nano 2018, 12, 6612. [PubMed: 29932670]

[11]. Latour G, Robinet L, Dazzi A, Portier F, Deniset-Besseau A, Schanne-Klein M-C, Sci. Rep 2016, 6, 26344. [PubMed: 27194180]

[12]. Morsch S, van Driel BA, van den Berg KJ, Dik J, ACS Appl. Mater. Interfaces 2017, 9, 10169. [PubMed: 28256818]

[13]. Lahiri B, Holland G, Centrone A, Small 2013, 9, 439. [PubMed: 23034929]

[14]. Ramer G, Aksyuk VA, Centrone A, Anal. Chem 2017, 89, 13524. [PubMed: 29165992]

[15]. Verbiest GJ, Rost MJ, Nat. Commun 2015, 6, 6444. [PubMed: 25753109]

[16]. Tuteja M, Kang M, Leal C, Centrone A, Analyst 2018, 143, 3808. [PubMed: 29878001]

[17]. a) Snyder RG, Scherer JR, Gaber BP, Biochimica et Biophysica Acta (BBA) - Biomembranes 1980, 601, 47; [PubMed: 7407164] b) Centrone A, Hu Y, Jackson AM, Zerbi G, Stellacci F, Small 2007, 3, 814. [PubMed: 17410617]

[18]. Baij L, Hermans JJ, Keune K, ledema P, Angew. Chem. Int. Ed 2018, 57, 7351.
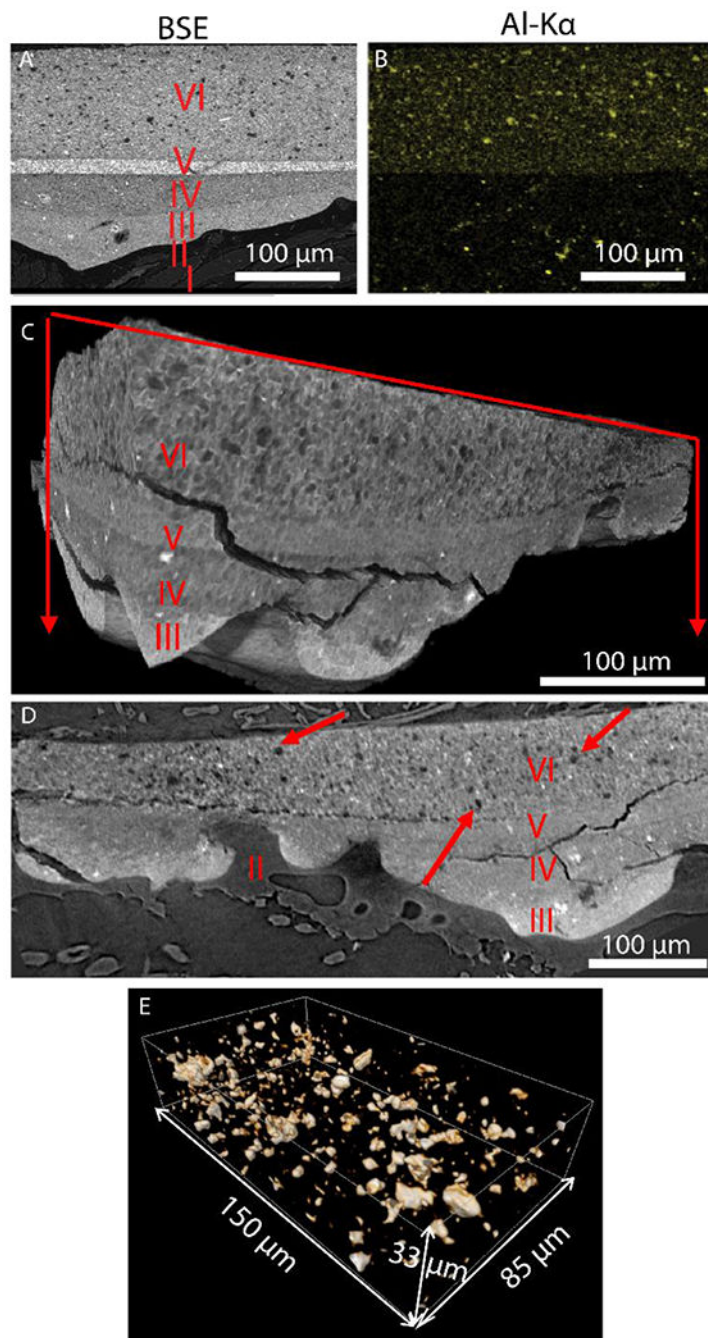
Figure 1.
A) BSE image of P250, B) EDX map of Al, C-F) μ-CT analysis of P250, C) A grayscale map has been applied to show the range of linear absorption coefficients, D) a slice through the volume shown in C showing low density (dark) regions dispersed throughout the paint layer, E) 3-D visualization of low-density regions in layer VI. Visualization was performed with volume rendering that shows higher X-ray absorbing materials transparent and lower absorbing materials opaque.
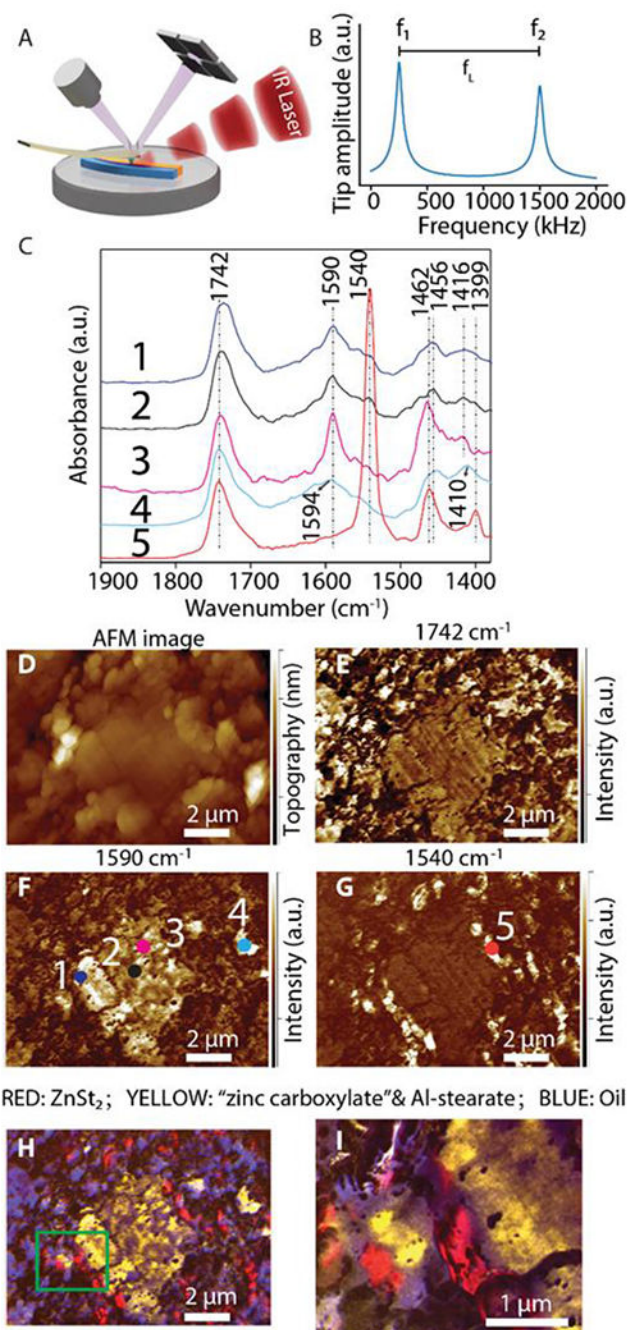
Figure 2.
A) PTIR setup schematic, B) Tapping PTIR scheme, C-I) PTIR analysis of a low-density region: C) PTIR spectra at the color-coded marked locations in F and G (points 1-5), the spectra were normalized to the ester band at 1742 cm^{-1} and offset for comparison, D) AFM topography. PTIR absorption maps at E) 1742 cm^{-1}, F) 1590 cm^{-1} and G) 1540 cm^{-1}, H) Reconstructed qualitative color-coded image of PTIR absorption intensity: $ZnSt_2$ (G, red), "zinc carboxylate" plus Al-stearate (F, yellow) and oil (E, blue). Colours are not displayed

on a common intensity scale, I) Higher resolution image of the area delimited by the green box in H, see Figure S8 for original maps.
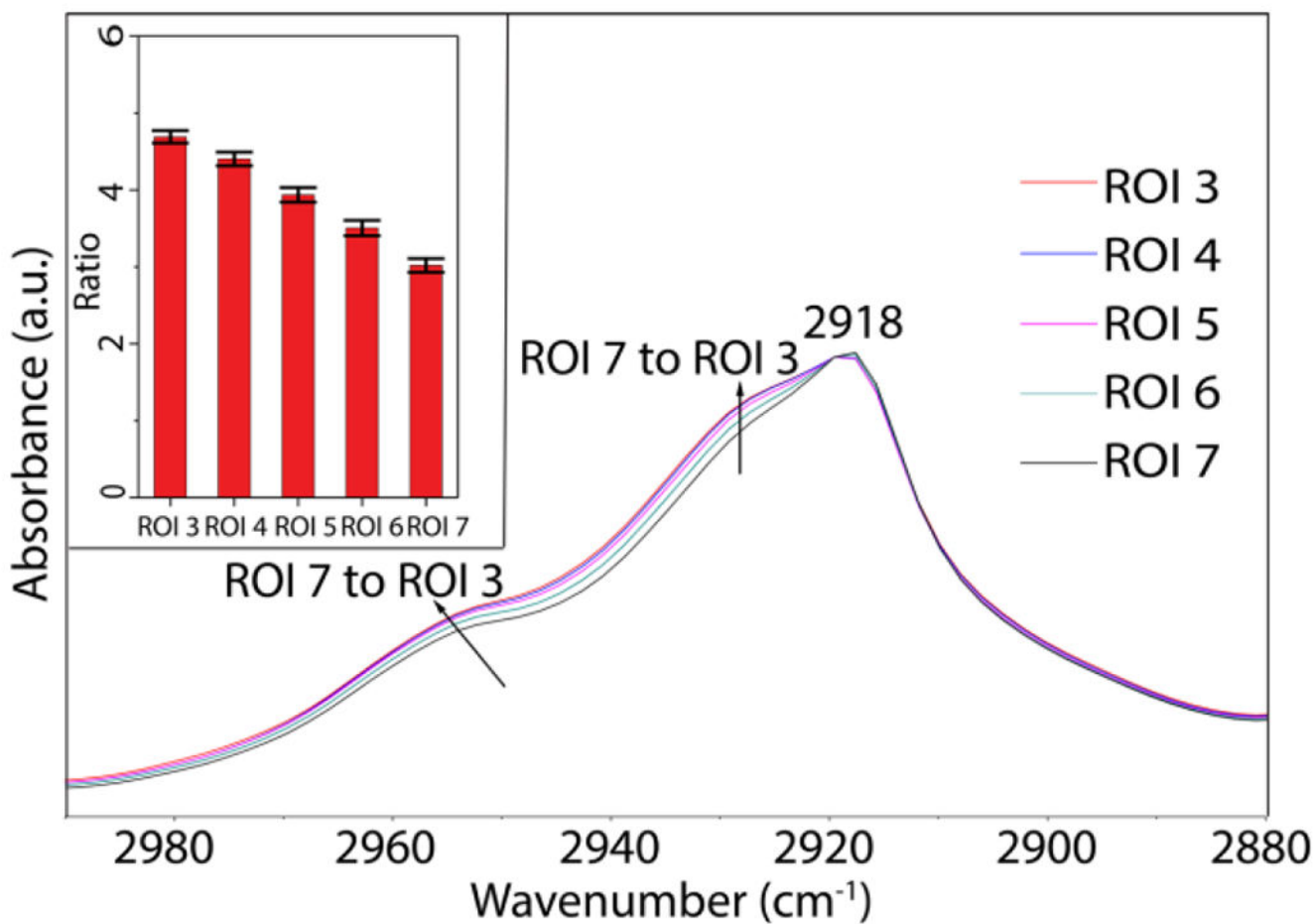
Figure 3.
Spectra from ROI 3 to ROI 7 in the C-H stretching region normalized to the CH_2 asymmetric stretching at 2918 cm^{-1}. Inset figure: ratio of the "zinc carboxylate" / ZnSt$_2$ peak area. The error bars represent a single standard deviation in calculating the area ratio and were determined by propagating the uncertainty due to the deconvolution of the individual carboxylate peak areas.